

# Chemical Science



**Accepted Manuscript** 

This article can be cited before page numbers have been issued, to do this please use: W. Huang, C. Wei, Y. Zhu, Q. Zhang and Z. He, *Chem. Sci.*, 2025, DOI: 10.1039/D5SC07119D.



This is an Accepted Manuscript, which has been through the Royal Society of Chemistry peer review process and has been accepted for publication.

Accepted Manuscripts are published online shortly after acceptance, before technical editing, formatting and proof reading. Using this free service, authors can make their results available to the community, in citable form, before we publish the edited article. We will replace this Accepted Manuscript with the edited and formatted Advance Article as soon as it is available.

You can find more information about Accepted Manuscripts in the <u>Information for Authors</u>.

Please note that technical editing may introduce minor changes to the text and/or graphics, which may alter content. The journal's standard <u>Terms & Conditions</u> and the <u>Ethical guidelines</u> still apply. In no event shall the Royal Society of Chemistry be held responsible for any errors or omissions in this Accepted Manuscript or any consequences arising from the use of any information it contains.



View Article Online DOI: 10.1039/D5SC07119D

#### **ARTICLE**

Received 00th January 20xx. Accepted 00th January 20xx

DOI: 10.1039/x0xx00000x

### Observation of Thermally-Activated Intersystem Crossing in Room-Temperature Phosphorescence of Weakly Donor-Acceptor-Donor π-Ternary Molecules

Wenbin Huang,<sup>a</sup> Chenlong Wei,<sup>b</sup> Yuxin Zhu,<sup>b</sup> Qian Zhang\*<sup>a</sup> and Zikai He\*<sup>a,b,c</sup>

The direct observation of thermally-activated intersystem crossing (TA-ISC) processes in room-temperature phosphorescence (RTP) has not been well investigated. Here, we reported four weakly donor-acceptor-donor π-ternary molecules featuring isomerism-dependent phosphorescence behaviors. The isomerism was modulated by changing the substitution position, offering tunable molecular planarity and  $\pi$ -conjugation. As a result, regulated energy levels and orbital configurations of the excited states facilitate additional TA-ISC channels as revealed by theoretical investigations. The temperature-dependent photoluminescence and fs- and ns-transient absorption spectra undoubtedly demonstrate their existence and effectiveness in promoting the efficient and persistent RTP. The ISC rate constant achieves a breakthrough of up to 1.93×109 s-1 within poly(vinyl alcohol) matrix film, surpassing that in many existing afterglow systems containing heavy or hetero atoms. Abundant triplet excitons are populated and enable remarkable room-temperature phosphorescence performance, facilitating potential applications in constructing thermosensitive glasses and anti-counterfeiting patterns. This study offers a practical mechanism for developing novel RTP materials.

#### Introduction

Purely organic room-temperature phosphorescence (RTP) has emerged as a rapidly developing area in the field of organic functional materials<sup>1-3</sup>. Benefiting from long-lived excitons, RTP materials demonstrate promising applications including bioimaging, X-ray scintillators, dynamic anti-counterfeiting systems, luminescent 3D-printed constructs, and beyond<sup>4-9</sup>. However, achieving efficient RTP remains a pivotal challenge for purely organic phosphors due to intrinsically weak spin-forbidden intersystem crossing (ISC), which determines the upper limit of phosphorescence efficiency<sup>10, 11</sup>. It is highly desirable to develop practical spin-flipping principles and call for molecular design strategies to ensure the efficient ISC process<sup>12-</sup>

Recently, several rational strategies were employed to enhance spin-orbit coupling (SOC) and increase ISC efficiency, including the well-known El-Sayed rule15, heavy-atom effect16, energy gap law17, hyperfine coupling<sup>18, 19</sup>, aggregation-induced level splitting<sup>20, 21</sup>, through-space SOC<sup>22</sup>, second-order spin-vibronic coupling<sup>23</sup>, energy transfer<sup>24-26</sup>, and others<sup>27-37</sup>. Each strategy can not only effectively promote ISC channels but also creatively put forth new RTP families. However, drawbacks such as the photodegradation introduced by heteroatoms<sup>38</sup> and the nonradiative decay process accelerated by

heavy-atoms<sup>39</sup> cannot be ignored. Given the importance and inconvenience of these strategies, it is of great significance to explore novel ISC principles for constructing new phosphorescent frameworks<sup>40</sup>.

As well known, thermally-activated reverse ISC based on donoracceptor structures has catalyzed the rapid development of the 3<sup>rd</sup> generation of OLED materials with thermally-activated delayed fluorescence feature<sup>41, 42</sup>. On the other hand, as a counterpart, the thermally activated forward ISC (TA-ISC) principle and related purely organic RTP have not been well investigated<sup>43</sup>. Several studies empirically adopt a threshold of 0.3 eV for the energy gap between  $S_1$  and  $T_n$  states to presume both normal and thermally activated ISC<sup>44, 45</sup>. However, compelling experimental evidence supporting endothermic TA-ISC processes from S<sub>1</sub> to higher-lying T<sub>n</sub> states (E(T<sub>n</sub>) > E(S<sub>1</sub>)) in purely organic RTP systems remains notably inadequate<sup>46</sup>. The reason may be that the reported systems have fewer TA-ISC transition pathways and weaker spin-orbit coupling, leading to their minor contribution, which has consequently not received much attention<sup>43, 45, 47</sup>. This demonstrates that enhancing the contribution of TA-ISC to the overall ISC process and exploring its potential roles hold promise for highlighting the importance of TA-ISC in the research of transition mechanisms. Modulation of the donoracceptor architecture and control of the excited-state energy levels are expected to elucidate the excited-state pathway and regulatory mechanism of TA-ISC48-50.

Herein, we developed a weakly donor-acceptor-donor (D-A-D) πternary system endowing varied molecular structures, tunable electronic configurations, adjustable energy levels, and persistent RTP<sup>51</sup>. Crucially, modulation of structural planarity was revealed to trigger additional TA-ISC pathways by increasing molecular conjugation and decreasing upper-lying triplet excited states. The  $\pi$ -

<sup>&</sup>lt;sup>a.</sup> School of Materials Science and Engineering, Harbin Institute of Technology Shenzhen, Shenzhen, Guangdong 518055, China

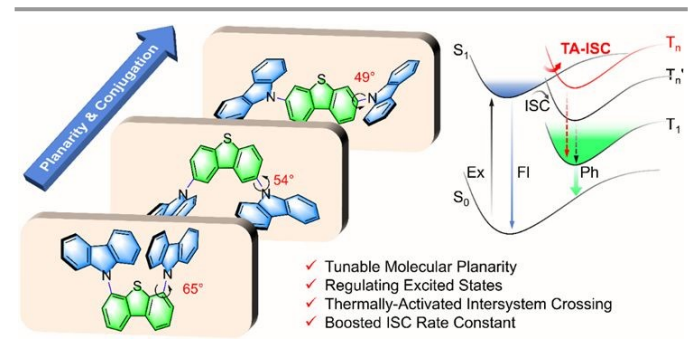
b. School of Science, Harbin Institute of Technology Shenzhen, Shenzhen, Guanadona 518055, China.

<sup>&</sup>lt;sup>c.</sup> School of Chemical Engineering and Technology, Harbin Institute of Technology, Harbin, Heilongjiang 150001, China.

Supplementary Information available: [details of any supplementary information available should be included here]. See DOI: 10.1039/x0xx00000x

ARTICLE Journal Name

conjugation and structural planarity of the isomers were modulated by adjusting the twisting dihedral angles, which were regulated via the connection position between the electron donor (carbazole) and the compared weak electron acceptor (dibenzothiophene) (Scheme 1). The excited states were then meticulously regulated. Suitable energy levels and orbital configurations of the excited states facilitate additional TA-ISC channels as revealed by theoretical investigations. The temperature-dependent photoluminescence and fs- and ns-transient absorption spectra undoubtedly demonstrated the existence and effectiveness of TA-ISC channels in promoting the efficient and persistent RTP. Notably, the ISC rate constant achieved a breakthrough of up to 1.93×109 s<sup>-1</sup> within poly(vinyl alcohol) film, surpassing those in typical afterglow systems containing heavy or hetero atoms<sup>27, 52, 53</sup> and facilitating abundant triplet exciton generation. With a nonradiative-decay-inhibited rigid environment, efficient RTP performance endowed the potential applications in constructing thermosensitive glasses and anti-counterfeiting luminescent patterns.



**Scheme 1** | Diagram of molecular structural engineering and the impact of enhanced-planarity and conjugation on intersystem crossing for achieving efficient organic RTP within a donor-acceptor-donor ternary  $\pi$ -conjugated framework.

#### **Results and Discussions**

This article is licensed under a Creative Commons Attribution-NonCommercial 3.0 Unported Licence

Open Access Article. Published on 10 November 2025. Downloaded on 11/11/2025 6:01:23 PM.

**Scheme 2** | Synthetic route and chemical structures of investigated ternary  $\pi$ -conjugated molecules

In our previous work, we first proposed that the weakly D-A structure could facilitate efficient SOC through endowing a moderate singlet-

triplet energy gap ( $\Delta E_{ST}$ ) and enhancing the LE character of excited states. <sup>51</sup> According to the energy gap law, small  $\Delta E_{ST}$  benefits for both forward and reverse nonradiative ISC. Strongly D-A structure results in the nearly degenerated lowest singlet (S<sub>1</sub>) and triplet (T<sub>n</sub>) excited states ( $\Delta E_{ST} \sim 0$  eV). It is powerful in constructing thermally-activated delayed fluorescence but not suitable for designing an efficient RTP system, because phosphorescence competes with the reverse ISC process. The weakly D-A structure can split the degenerated S<sub>1</sub> and T<sub>n</sub> state (moderate  $\Delta E_{ST}$ ) to block the reverse ISC process. Moreover, a weakly D-A  $\pi$ -conjugated architecture endows the tuneable hybridized orbit configurations with charge-transfer (CT) and locally-excited characteristics, allowing the El-Sayed rule and second-order vibronic coupling mechanism to work.

Following the strategy, four D-A-D molecules with different substitution modes were designed and synthesized following the procedures in Scheme 2. Carbazole (Cz) was used as the electronic donor, and dibenzothiophene (DBT) was used as the weakly electronic acceptor. The electronic donor and acceptor were assigned based on their relative electronic properties when linked within one molecular architecture, rather than their absolute electronic features. It was worth noting that Cz was lab-synthesized through a one-step coupling reaction from 2-bromodiphenylamine<sup>54,</sup> 55 to exclude the well-known impurity. The targeted compounds were synthesized via Ullmann coupling with moderate yields. Based on the substitution position on DBT, four molecules were named as 4,6-DCzDBT, 2,8-DCzDBT, 3,7-DCzDBT, and 2,7-DCzDBT, respectively. The structural characterizations and HPLC measurements were included in the Supporting Information. Further experimental details are available in the Supporting Information.

#### **Photophysical Properties.**

The absorption and luminescence spectra were measured to investigate the photophysical properties. As depicted in Figure 1a, the overall absorption profiles of four  $\pi$ -ternary molecules were similar, with a bathochromic shift at around 340 nm corresponding to S<sub>1</sub> states. It suggested an excitation intermolecular charge transfer transition from the Cz segment to the partially conjugated DBT part. The situation aligned with the calculated HOMOs (mainly distributed at Cz units) and LUMOs (distributed at DBT units), as shown in Figure S1, ESI $^{\dagger}$ . The weakly D-A-D  $\pi$ -ternary molecular architectures were also confirmed. The absorption spectra reflected an apparent superposition of Cz and DBT segments, together with enhanced molar absorption coefficients and redshifted onset absorption wavelengths. Specifically, 3,7-DCzDBT exhibits the longest absorption wavelength and the highest molar absorption coefficient corresponding to the S<sub>1</sub> excitation, indicating its superior molecular  $\pi$ -conjugation. In contrast, 4,6-DCzDBT displays the shortest absorption wavelength, indicating its poorest molecular πconjugation.

Subsequently, the steady-state and delayed photoluminescence (PL) spectra were recorded in Figure 1b. The room-temperature PL spectra displayed broad emission without vibrational progressions in contrast to the well-resolved emission profiles of Cz and DBT segments, due to the intramolecular charge-transfer (¹CT) characteristics of the excited states. The nanosecond lifetimes confirmed the fluorescence nature (Table S5, ESI†). It was worth noting that in

Journal Name ARTICLE

View Article Online DOI: 10.1039/D5SC07119D

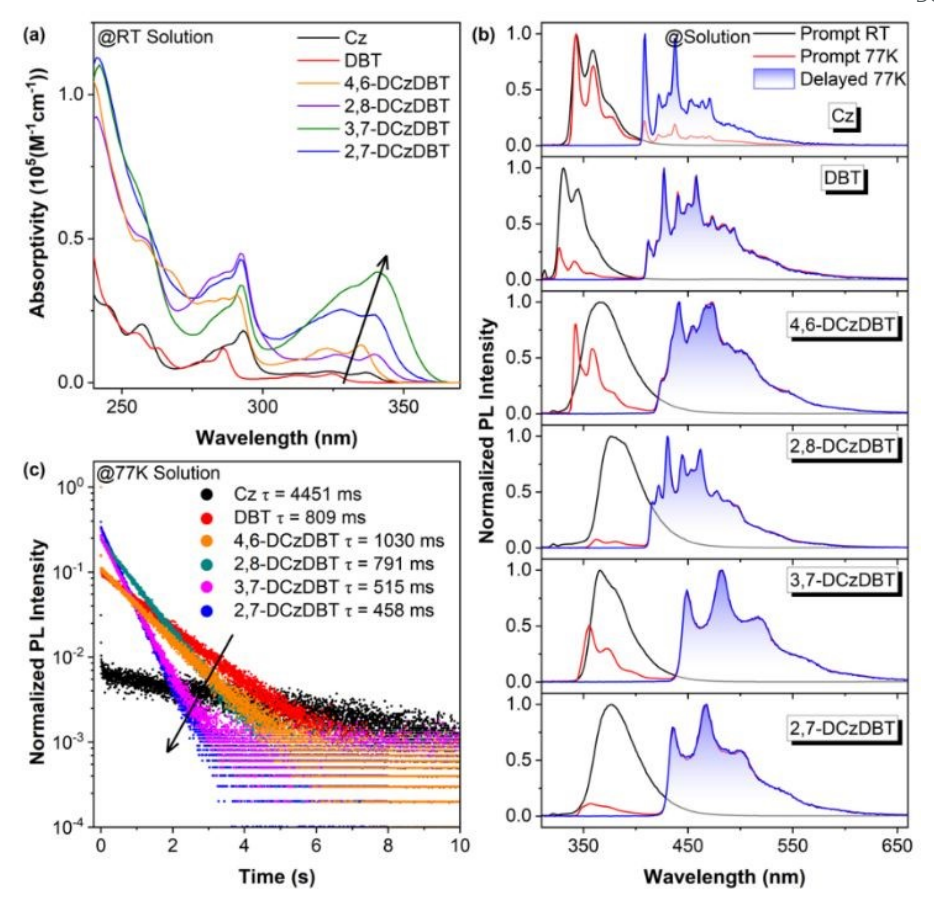


Figure 1 | (a) UV-visible absorption spectra at room temperature (RT), (b) normalized PL prompt at RT, normalized PL prompt and delayed (1 ms) spectra at 77 K under 293 nm excitation, (c) time-resolved phosphorescent decay curves of Cz, DBT, 4,6-DCzDBT, 2,8-DCzDBT, 3,7-DCzDBT, and 2,7-DCzDBT in 2-MeTHF (10-5 M) at 77 K.

different solutions, the PL exhibited a polarity-dependent redshift emission behaviour, indicating that their <sup>1</sup>CT characteristics of S<sub>1</sub> (Figure S2, ESI<sup>+</sup>). Combined with the fact that the absorption spectra were hardly affected by the solvent polarity, the molecules enjoyed a weakly D-A-D feature at ground state (Figure S3, ESI†). It also agreed with their slightly different electronic properties of the Cz and DBT segments. When the temperature decreased to 77 K, the fluorescence emission emerged with multiple vibrational peaks similar to Cz, indicating that the fluorescence mainly originated from the Cz segments. As the temperature decreases, the conformational adjustment and feasible relaxation to a stable CT state is hindered; thus, under 77 K the system tends to exhibit the locally-excited (LE) state with vibrational PL characteristics. Simultaneously, prominent and vibrational phosphorescence emission bands emerged in the range of 420-650 nm, with lifetimes in the second range (Figure 1c and Table S5, ESI†). Comparing subtle vibrational profiles (Figure 1b) and lifetimes (Figure 1c), it was confirmed that the phosphorescent emissions were similar to that of the DBT segment, indicating that T1 was characterized by a dominating  $(\pi,\pi^*)$  configuration contributed by the DBT segment. The weaker vibrational progressions and short persistent lifetimes in 3,7-DCzDBT and 2,7-DCzDBT were

consistent with their better molecular π-conjugation. Additionally, a boosted phosphorescence proportion (the ratio of the phosphorescence emission area to the total PL spectra area) and the enhanced LE characteristics in excited states at 77 K were found in 2,8-DCzDBT and 2,7-DCzDBT, suggesting a higher ISC efficiency (Figures S4 and S5, ESI†). Furthermore, the higher triplet energy level of 2,8-DCzDBT suggests that it could serve as a candidate for deep-blue emissive materials<sup>56</sup>. Notably, 2,7-DCzDBT combined the high phosphorescence ratio characteristic of 2,8-DCzDBT with a phosphorescence profile analogous to 3,7-DCzDBT. This demonstrated that strategic positional isomerism effectively modulated RTP performance.

After conducting fundamental photophysical property investigations in solutions, further studies were conducted on their RTP performance by polymer matrix hosting. We selected poly(vinyl alcohol) (PVA) as a rigid matrix to provide an environment for suppressed nonradiative decay, where sufficient hydroxyl groups and hydrogen bond networks inhibit intra- and intermolecular motions to trigger intrinsic molecular RTP emission  $^{57-60}$ . The optimal doping mass concentration was selected as 1:1000 of  $m_{\rm Guest}$ :  $m_{\rm PVA}$ , and as-prepared films were subjected to photothermal treatments to remove molecular oxygen and water and ensure matrix rigidity upon

emical Science Accepted Manuscript

View Article Online DOI: 10.1039/D5SC07119D

#### **ARTICLE**

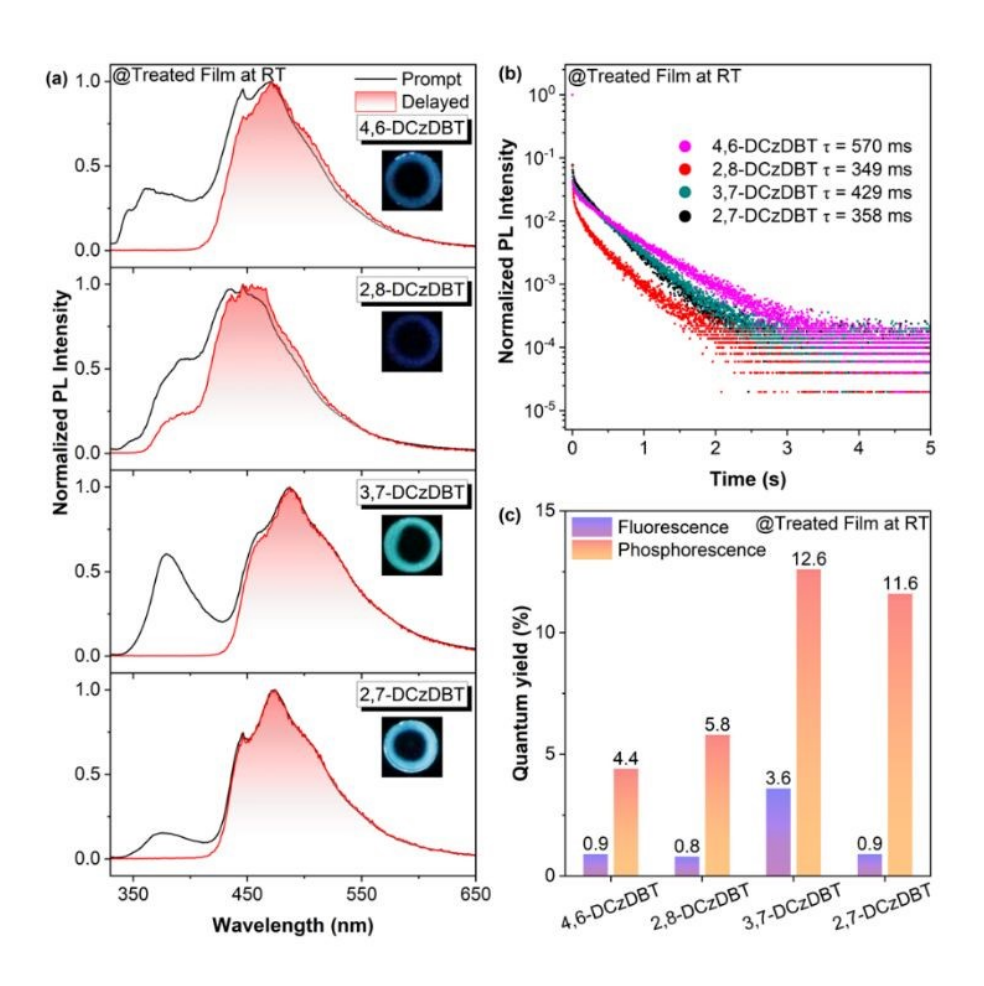


Figure 2 | (a) Normalized PL spectra and delayed (1 ms) spectra, (b) time-resolved phosphorescent decay curves, and (c) fluorescence and phosphorescence quantum yields under ambient conditions of treated PVA films with doped 4.6-DCzDBT, 2.8-DCzDBT, 3.7-DCzDBT, and 2.7-DCzDBT, Inset; photographs taken after the removal of the UV excitation source of 254 nm under ambient conditions of treated PVA films.

crosslinking (Figures S6 and S7, ESI+). The PL performance of treated PVA films was significantly improved, as illustrated in Figure 2. Intense and persistent RTP was achieved, ascribing to the environmental rigidification. The treated films exhibit typical unimolecular emission behaviours, similar to those observed in their low-temperature solutions, but with fewer vibrational progressions. The PVA films exhibited a similar fluorescence emission band at ~370 nm, but their phosphorescence emission differed, as illustrated by the inset pictures in Figure 2a and the CIE coordinates in Figure S8, ESI†. Unexpectedly, in contrast to the high phosphorescence ratio observed under low-temperature conditions, it is striking that 2,8-DCzDBT failed to exhibit satisfactory RTP performance. 3,7-DCzDBT and 2,7-DCzDBT exhibited outstanding afterglow performance, as confirmed by the highest quantum yield of up

to 12.6 % (Figure 2c), the longer lifetime of 429 ms, and the redshifted emission wavelength in 3,7-DCzDBT films. The decay rate constants were calculated (Table S7, ESI+), revealing that the nonradiative decay rate constants ( $k_{NR}$ ) are close for these treated PVA films, but the ISC rate constants ( $k_{\rm ISC}$ ) are distinguishable and responsible for the differentiated phosphorescence efficiencies. Notably, 3,7-DCzDBT exhibits an extremely high  $k_{\rm ISC}$  of up to  $1.93 \times 10^9$  s<sup>-1</sup>, a value rarely reported in purely organic RTP systems<sup>22, 27, 52, 53</sup>.

#### **Theoretical Calculations**

To gain deep insights into the underlying mechanism, theoretical calculations on these molecules were performed (Figure 3). The presented natural transition orbitals (NTOs) revealed that all molecules exhibited typical D-A-D characteristics of S<sub>1</sub> state, with bilateral carbazoles acting as

View Article Online DOI: 10.1039/D5SC07119D

#### **ARTICLE**

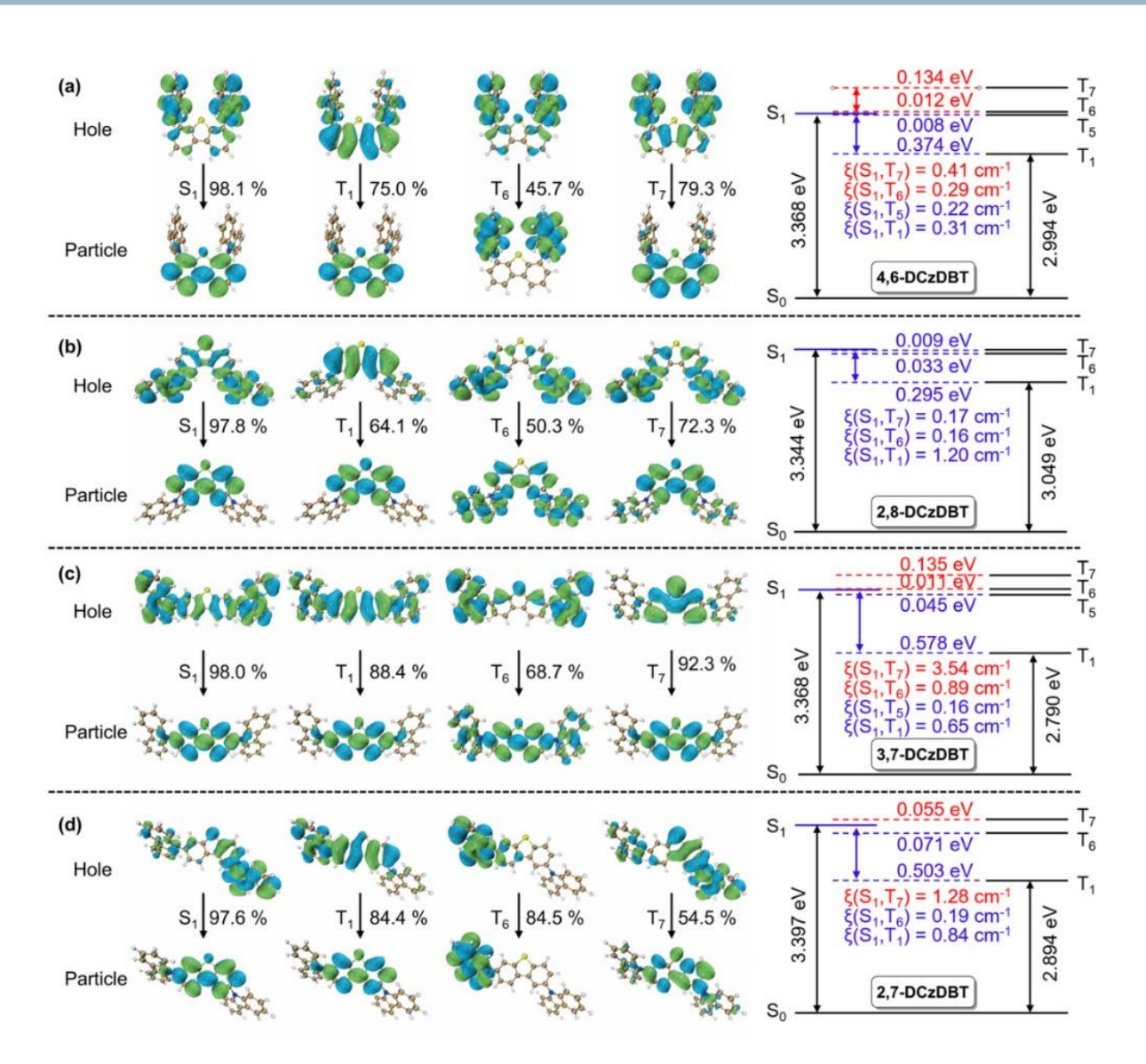


Figure 3 | The calculated natural transition orbitals of the frontier excited singlet and triplet states, the state-energy-level diagrams, and the SOC coefficients (ξ) for (a) 4,6-DCzDBT, (b) 2,8-DCzDBT, (c) 3,7-DCzDBT, and (d) 2,7-DCzDBT in the monomeric state at (TD)-B3LYP/def2-SVP level.

donors (hole) and the middle dibenzothiophene serving as acceptor (particle). As illustrated in Figure 3 (left), the NTOs of  $S_1$  exhibited a main  $^1$ CT character with a certain extent of  $^1$ LE features, demonstrating the typical hybridized  $^1$ CT and  $^1$ LE nature. Concerning  $T_1$  states, NTOs showed good orbital overlaps between holes and particles. The excited state configuration of  $T_1$  was dominated by the  $^3$ LE character with little  $^3$ CT feature involved. The calculation results matched well with UV-Vis absorption and PL spectra profiles. Depending on the molecular structure ( $\pi$ -conjugation), the configuration

differentiation between  $S_1$  and  $T_1$  can enhance the probability of the ISC transition, following El-Sayed's rule<sup>61</sup>. Notably, 2,8-DCzDBT has a distinct difference between the  $S_1$  ( $n,\pi^*$ ) and  $T_1$  ( $\pi,\pi^*$ ) states, resulting in a good  $\xi(S_1,T_1)$  value of 1.20 cm<sup>-1</sup> (Figure 3b). However, 3,7-DCzDBT has the highest similarity of NTOs between the  $S_1$  and  $T_1$  states and thus a poor  $\xi(S_1,T_1)$  value of 0.65 cm<sup>-1</sup> (Figure 3c). Additionally, energy gaps between  $S_1$  and  $T_1$  ( $\Delta E_{ST}$ ) indicate that the smallest  $\Delta E_{ST}$  exists in 2,8-DCzDBT. Hence, 2,7-DCzDBT and 2,8-DCzDBT have stronger SOC  $\xi(S_1,T_1)$  values than those of 3,7-DCzDBT and 4,6-DCzDBT. The

Shemical Science Accepted Manus

ARTICLE Journal Name

efficient ISC was consistent with their high phosphorescence proportion in the overall PL spectra of solutions at 77 K (Figure 1b and S5, ESI<sup>+</sup>).

However, upon recovering to room temperature, the RTP performance situation reversed, with 3,7-DCzDBT exhibiting outstanding afterglow performance. Therefore, further screening of the closed-lying triplet states was considered (lower than the energy level of S2), and the possible TA-ISC processes involving multiple  $S_1 \rightarrow T_n$  transition channels were found in these derivatives (Figure 3 and Table S8, S9, ESI+). Interestingly, several high SOC values were found between the higher excited triplet states (T<sub>6</sub> or T<sub>7</sub>) and the S<sub>1</sub> state because the greater  $(\pi,\pi^*)$  character in the  $S_1$  state and the higher  $(n,\pi^*)$ components in the T<sub>6</sub> and T<sub>7</sub> states are conducive to the ISC process. For example, 3,7-DCzDBT had two high-lying triplet excited states, T<sub>6</sub> (3.379 eV) and T<sub>7</sub> (3.503 eV), which were higher than S<sub>1</sub> (3.368 eV). The conspicuous NTO configurations of the main <sup>3</sup>LE feature in T<sub>6</sub> and T<sub>7</sub> supported the high values of  $\xi(S_1,T_6)$  of 0.89 cm<sup>-1</sup> and  $\xi(S_1,T_7)$  of 3.54 cm<sup>-1</sup>, respectively, despite the thermodynamically unfavourable requirements (Figure 3c). Considering the better RTP performance of 3,7-DCzDBT and 2,7-DCzDBT, it was speculated that the high-lying triplet states of T<sub>7</sub> and T<sub>6</sub> should contribute to the overall ISC process at room temperature by providing multiple transition channels with enhanced SOCs, which were absent in 2,8DCzDBT. The endothermic process of TA-ISC from the State to the high-lying triplet states had not been experimentally verified in RTP systems, despite occasionally mentioned 2. The photophysical properties and calculation results inspired the possibility of involvement with the high-lying triplet states in ISC. Therefore, it needed to conduct the temperature-dependent deep photophysical investigations by monitoring the dynamic behaviours of excited states.

#### **Temperature-dependent Photoluminescence**

As depicted in Figures 4a and Figures 4c top, the PL spectra of the 3,7-DCzDBT doped PVA films exhibited significant temperature-dependent phosphorescence behaviours. As the temperature increased, the phosphorescence intensity initially increased from 80 to 120 K and then decreased from 140 to 320 K. It reached a maximum at 120 K by monitoring the 487 nm emission. The reduced tendency upon increasing temperature was understandable because of the thermally enhanced nonradiative decay ( $k_{\rm NR}$ ). However, the increased tendency from 80 to 120 K was unexpected. Considering the extremely low temperature and effectively restricted molecular motions, the  $k_{\rm NR}$  should be pretty small and do not significantly affect within the temperature range of 80–120 K. Therefore, the increased tendency could be attributed to the TA-ISC process and thus boost triplet exciton generation. This phenomenon

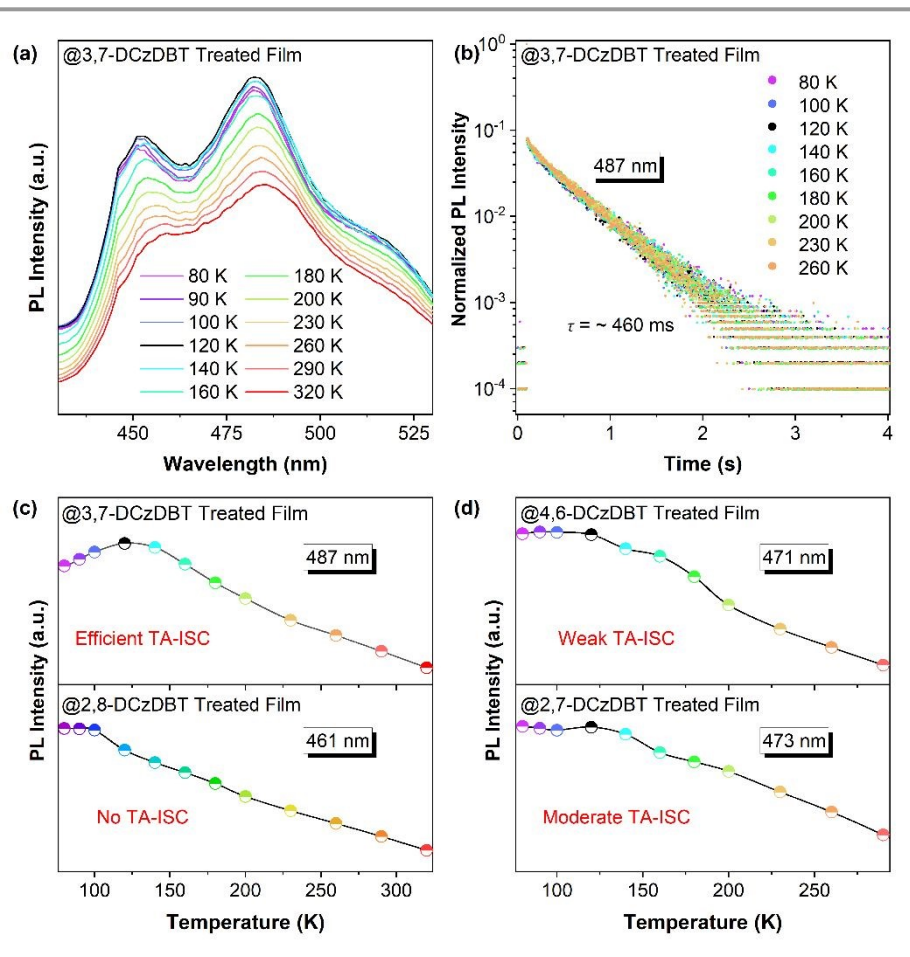


Figure 4 | (a) Phosphorescence spectra and (b) time-resolved phosphorescent decay curves at different temperatures of treated PVA films with doped 3,7-DCzDBT. The emission intensity of maximum emission peaks at different temperatures of (c) 3,7-DCzDBT and 2,8-DCzDBT, and (d) 4,6-DCzDBT and 2,7-DCzDBT.

View Article Online DOI: 10.1039/D5SC07119D

#### **ARTICLE**

Is similar to the "hot triplet exciton" model observed in highlying reverse intersystem crossing process<sup>63-65</sup>. Moreover, the same phosphorescence decay curves at different temperatures eliminated the possible interferences from the anti-Kasha upper-level triplet emissions (Figure 4b).

As shown in Figure S9b, ESI<sup>+</sup> and Figure 4c bottom, it was observed that the phosphorescence of 2,8-DCzDBT gradually became weakened with increasing temperature, and no trend of transformation was observed. It agreed with the calculation results that there were no closed upper-lying triplet states (Figure 3b). The apparent difference in temperature-dependent intensity trends between 3,7-DCzDBT and 2,8-DCzDBT strongly demonstrated that thermal activation played an essential role in ISC. Moreover, 4,6-DCzDBT was investigated for comparison with 3,7-DCzDBT to validate the TA-ISC process (Figure 4d), which had a similar energy gap between S<sub>1</sub> and T<sub>7</sub> but different values. As the temperature decreased, phosphorescence intensity gradually increased due to the reduction of  $k_{NR}$ . However, around 150 K, a gentle downward slope appeared, indicating the involvement of upper-level triplet state T<sub>7</sub> in the ISC process. Unfortunately, the small SOC value  $\xi(S_1,T_7)$  exerted a weaker effect on the overall ISC process. The similar increased tendency was not observed (Figure S9a, ESI†). We also characterized the temperature-dependent PL spectra of 2,7-DCzDBT, as shown in Figure S9c, ESI† and Figure 4d bottom. Similar to 3,7-DCzDBT, the temperature-dependent phosphorescence intensity curve of 2,7-DCzDBT showed a trend shift around 120 K, which was consistent with the calculated results. The temperature-dependent PL spectra and calculated results consistently confirmed the existence of the TA-ISC process. The significant contribution of the upper-level triplet excited states in populating the emissive T<sub>1</sub> excitons was revealed.

#### **Temperature-dependent Transient Absorption**

To elucidate the underlying photophysical mechanisms of the singlet-triplet transition, we employed transient absorption (TA) spectroscopy to probe the excited-state evolution dynamics of the representative 2,8-DCzDBT and 3,7-DCzDBT<sup>66,</sup> femtosecond transient absorption measurements revealed a positive signal at 500-700 nm for both systems (Figures 5a and 5b), indicative of excited-state absorption (ESA) corresponding to  $S_1 \rightarrow S_n$  transitions. TA wavelength kinetic traces were extracted to resolve the statespecific dynamics. For 3,7-DCzDBT, the ESA signal reached its maximum intensity within 594 fs and decayed with the S<sub>1</sub> relaxation, consistent with its fluorescence lifetime as monitored at 575 nm ( $\tau$  = 0.3 ns) (Figure 5c and Table S5, ESI†). An analogous decay was observed for 2,8-DCzDBT at 620 nm (Figure S10c, ESI+). Notably, a distinct transient signal rather

than noise emerged at ~1000 ps. Its intensity underwent the complete rise-decay profile and was found stronger when monitored at 650 nm than at 575 nm (Figure 5c inset). Later on, it was assigned to triplet-triplet absorption (TTA) from the upper-level  $T_7$  state with a nanosecond decay lifetime (~0.7 ns), indicating the presence of  $S_1 \rightarrow T_n$  TA-ISC transitions. There is no corresponding feature detected in 2,8-DCzDBT (Figure S10c, FSI†).

To elucidate the dynamics of triplet states, nanosecond transient absorption (ns-TA) spectroscopy was then performed on 2,8-DCzDBT and 3,7-DCzDBT (Figures 5d and 5g). Distinctly, 3,7-DCzDBT exhibited dual absorption bands around 400-500 (TTA@445nm) and 550-750 nm (TTA@650nm), respectively, in contrast to the one absorption band at 400–500 nm in 2,8-DCzDBT (TTA@430nm). Kinetic traces extracted from these bands displayed microsecond-scale decays, confirming triplet exciton-mediated processes and indicating their TTA features (Figures 5e, 5f, and 5h). Multi-exponential analysis revealed complex rise-decay profiles indicative of step relaxation. Cross-validation ns-TA with NTO calculations and photoluminescence data enabled dynamics assignments: For 3,7-DCzDBT's absorption at 650 nm (Figure 5e), an initial rise component ( $\tau = 0.7$  ns) directly signified  $S_1 \rightarrow T_7$  TA-ISC, being consistent with fs-TA ESA signal in Figure 5c and the calculated k<sub>ISC</sub> based on steady-state photophysical properties (1.93×10<sup>9</sup> s<sup>-1</sup> 1), followed by a rapid decay ( $\tau = 5.4$  ns) attributed to  $T_7 \rightarrow T_1$ internal conversion, culminating in a slow decay ( $\tau$  = 23.6  $\mu$ s) corresponding to  $T_1 \rightarrow S_0$  depopulation. The band corresponded to the TA from the upper level T<sub>7</sub> state. Analogous dynamics at 445 nm (Figure 5f) involved a slower  $S_1 \rightarrow T_6$  normal ISC ( $\tau = 1.7$ ns) with a subsequent  $T_6 \rightarrow T_1$  internal conversion ( $\tau = 13.6$  ns) and a  $T_1 \rightarrow S_0$  depopulation with a similar decay lifetime of 25.5 μs. Critically, ns-TA in Figure 5d confirmed  $S_1 \rightarrow T_7$  TA-ISC as the dominant evolution pathway in 3,7-DCzDBT, consistent with theoretical predictions.

In contrast, ns-TA of 2,8-DCzDBT at 430 nm (Figures 5g and 5h) demonstrated the evolution process of the  $S_1 \rightarrow T_6$  ISC ( $\tau = 2.5$  ns, notably longer than 0.7 ns in 3,7-DCzDBT), the  $T_6 \rightarrow T_1$  internal conversion, and the  $T_1 \rightarrow S_0$  depopulation ( $\tau = 38.2~\mu s$ ), with no spectroscopic evidence for upper-level  $T_7$  involvement. The kinetic difference that accelerated ISC and shortened  $T_1$  decay in 3,7-DCzDBT relative to 2,8-DCzDBT directly rationalized the observed different RTP behaviours. To further validate TAISC, temperature-dependent ns-TA measurements were conducted (Figures 5i and S10, ESI†). For 3,7-DCzDBT, the ns-TA signal intensity at 650 nm progressively diminished with decreasing temperature, indicating the suppressed to no  $S_1 \rightarrow T_7$  ISC channels at low temperature. No appreciable signal

ARTICLE Journal Name

variations occurred in 2,8-DCzDBT at 445 nm (Figure S10b, ESI<sup>+</sup>). Nevertheless, the cumulative evidence confirmed not only online

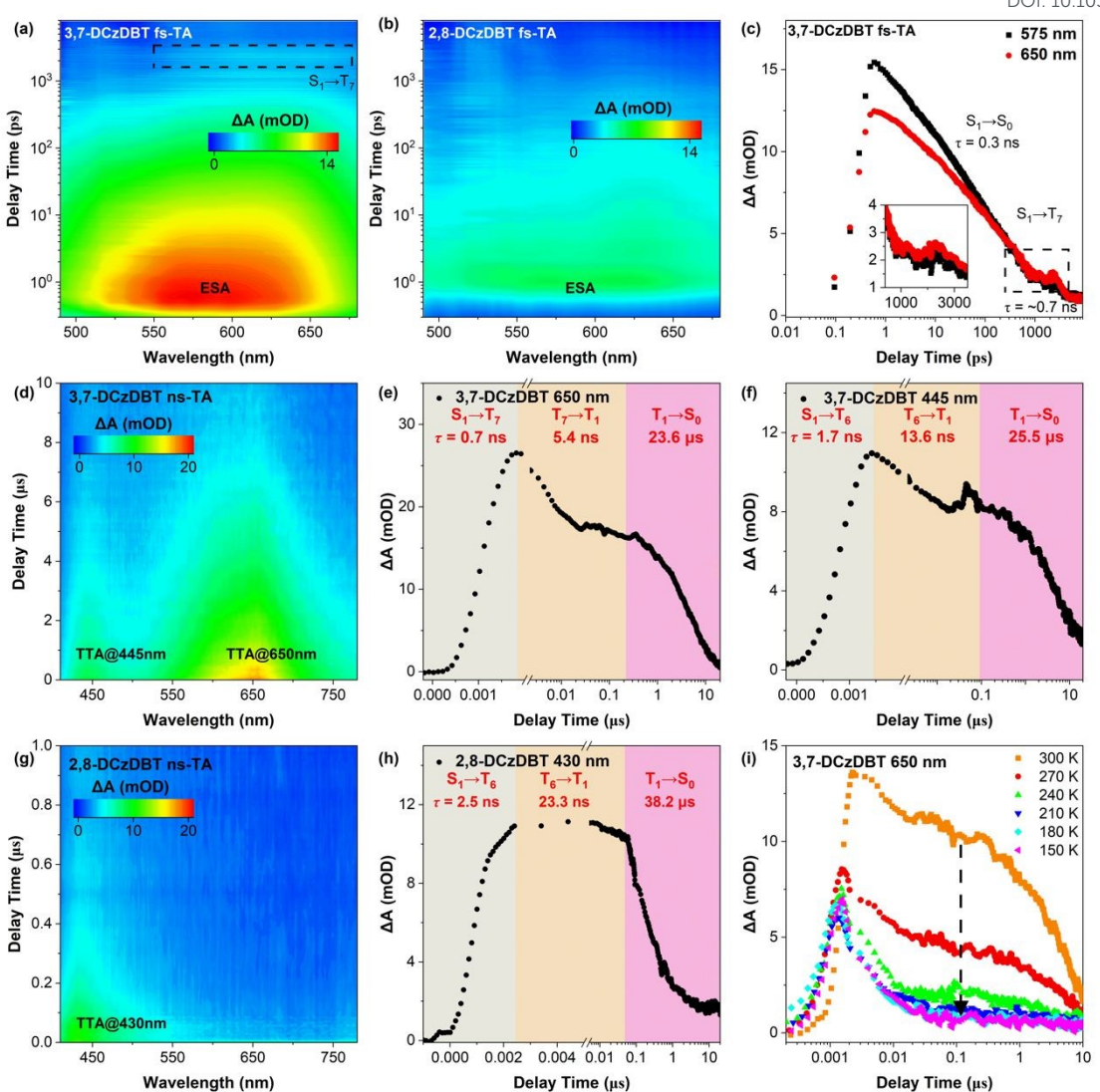


Figure 5 | Decay time-wavelength two-dimensional fs-TA color maps of (a) 3,7-DCzDBT and (b) 2,8-DCzDBT, and ns-TA color maps of (d) 3,7-DCzDBT and (g) 2,8-DCzDBT in 2-MeTHF (10<sup>-4</sup> M) at room temperature. (c) fs-TA dynamics detected at 575 and 650 nm in 3,7-DCzDBT. ns-TA dynamics detected at e) 650 nm and (f) 445 nm in 3,7-DCzDBT, and (h) 430 nm in 2,8-DCzDBT, respectively, with corresponding excited-state relaxation lifetimes. (i) ns-TA dynamics at different temperatures from 300 to 150 K detected at 650 nm in 3,7-DCzDBT. The pump light wavelength is 340 nm.

the existence of TA-ISC but also its superior capability of promoting ISC in 3,7-DCzDBT.

#### Structure-property Relationship

It is crucial to scrutinize the underlying structure-property relationship and formulate a rational molecular design strategy to develop TA-ISC RTP systems.  $\pi$ -Conjugation, the degree of  $\pi$ -electron delocalization, corresponds to the molecular planarity and substitution-dependent electronic effect in these polycyclic aromatic structures. Based on the extent of redshift absorption,

 $\pi\text{-conjugation}$  suggests an ordered and increased molecular planarity from 4,6-DCzDBT to 2,8-DCzDBT, 2,7-DCzDBT, and 3,7-DCzDBT. Their molecular configurations were then obtained by culturing single crystals and were doubly verified by theoretical calculations. As shown in Figure 6a, the calculated molecular structures closely resembled those of the single crystals, particularly in terms of the dihedral angles between the carbazole and dibenzothiophene units. The subtle discrepancies in the dihedral angles arise from the compression or

This article is licensed under a Creative Commons Attribution-NonCommercial 3.0 Unported Licence

Open Access Article. Published on 10 November 2025. Downloaded on 11/11/2025 6:01:23 PM

View Article Online DOI: 10.1039/D5SC07119D

#### **ARTICLE**

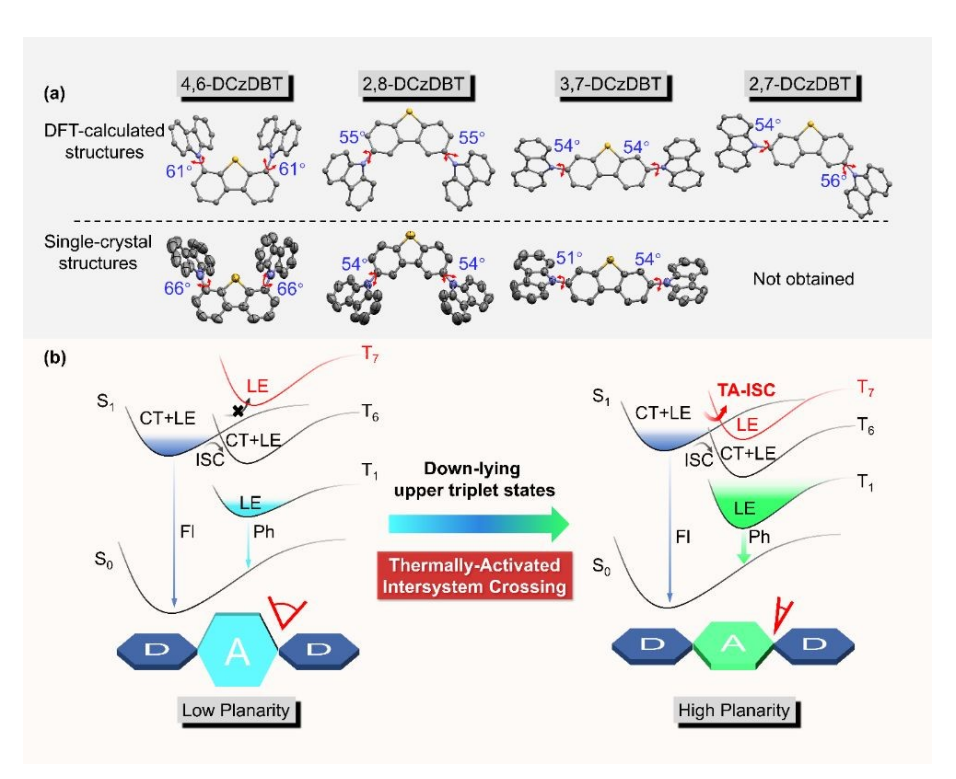


Figure 6 | (a) Single-crystal structures and density-functional theory (DFT) optimized structures of 4,6-DCzDBT, 2,8-DCzDBT, 3,7-DCzDBT, and 2,7-DCzDBT with average-calculated dihedral angles between carbazole and dibenzationhene units. (b) Scheme describing the thermally-activated ISC principle.

deformation of the molecular conformation within the unit cell due to intermolecular interactions. Notably, 4,6-DCzDBT possessed the largest dihedral angles, and 3,7-DCzDBT represented the smallest dihedral angles. The small dihedral angles indicated the high molecular planarity and  $\pi$ conjugation, which aligned with the redshifted emission wavelength and their superior RTP performance (Figure 2c). In detail, the high molecular planarity of 3,7-DCzDBT lowered energy levels of the upper triplet states through enhanced  $\pi$ conjugation, allowing upper-level T<sub>7</sub> to approach S<sub>1</sub> and facilitating the TA-ISC process. Additionally, enhanced  $\pi$ conjugation supported T<sub>7</sub> in endowing more <sup>3</sup>LE configurations on the central emitting DBT acceptor, and the <sup>3</sup>LE configuration promoted an efficient TA-ISC by fulfilling El-Sayed's rule between hybridized  $S_1$  ( ${}^1CT + {}^1LE$ ) and  $T_7$  ( ${}^3LE$ ). It was worth noting that 2,7-DCzDBT inherited partial structural and conjugation characteristics from its 2,8-DCzDBT and 3,7-DCzDBT counterparts, demonstrating an intermediate RTP performance in terms of lifetime (close to that of 2,8-DCzDBT) and efficiency (close to that of 3,7-DCzDBT) (Figure 2).

Therefore, the precise control of molecular  $\pi$ -conjugation in the weakly D-A-D system can sophisticatedly tune the ISC process and facilitate RTP performance accordingly. When a

large dihedral angle existed between the  $\pi$ -donor and  $\pi$ acceptor, the singlet and triplet excited states possessed weak SOC and insufficient ISC due to the same orbital configurations. Through enhancing structural planarity by reducing large dihedral angles, the delocalization within the donor-acceptor structure regulated the electronic configuration of excited states. The energy level of the upper triplet excited states was lowered, and the orbital configuration of the close-lying triplet state was converted. As a result, additional TA-ISC channels with high SOC values were facilitated, boosting RTP efficiency (Figure 6b). As a benefit, the high  $\pi$ -conjugation provided a relatively pure  $(\pi,\pi^*)$  configuration for  $T_1$ , guaranteeing a small radiative rate of phosphorescence and, consequently, a persistent RTP lifetime. These findings not only provide us with a clear and practical molecular design principle but also high-performance phosphors.

#### **Anti-counterfeiting and Thermal Sensing Applications**

Given the remarkable phosphorescence performance of these doped PVA films, we explored their applications in anticounterfeiting and thermal sensing as a proof-of-concept. As depicted in Figure 7a, treated PVA films containing 3,7-DCzDBT and 2,7-DCzDBT were utilized to construct a simple anti-

Journal Name

counterfeiting pattern of "HIT". Upon UV excitation, the luminescent pattern was observed. When the excitation ceased, an afterglow pattern of "HIT" persisted. Two seconds later, the pattern transformed to the "1111" pattern. In addition, a peach-shaped PVA film doped with 3,7-DCzDBT was soaked and affixed to the glass bottles, followed by a 40-minutes thermal treatment (Figure 7b). The prepared film was employed to monitor environmental temperature. It was observed that as the temperature increased (368 K), the colour gradually shifted to deep blue, and the brightness decreased. Subsequently, as the temperature dropped, the emission was restored to its initial state. The process can be repeated for several cycles.

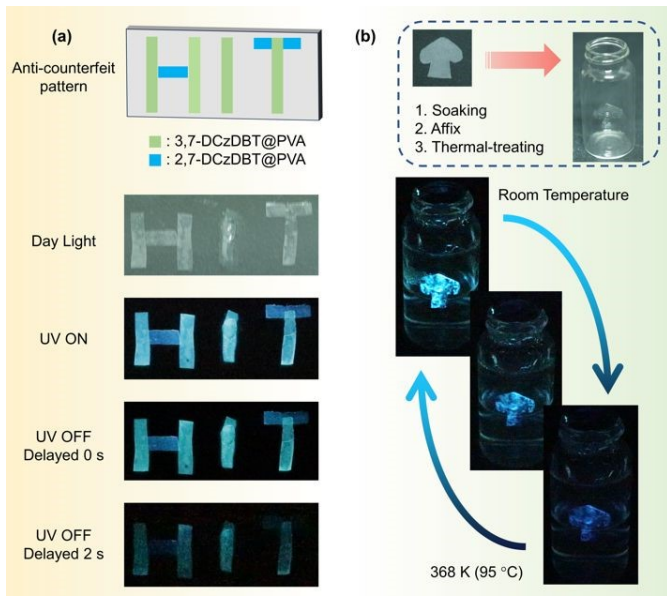


**Figure 7** | (a) Schematic diagram in preparation of anti-counterfeiting patterns and photographs of the security code before and after turning off the 254 nm UV lamp. (b) Schematic diagram in preparation of thermosensitive glasses with 3,7-DCzDBT film and pictures of thermal-sensing process from 368 K to 295 K under 254 nm UV lamp excitation

#### Conclusion

This article is licensed under a Creative Commons Attribution-NonCommercial 3.0 Unported Licence

Open Access Article. Published on 10 November 2025. Downloaded on 11/11/2025 6:01:23 PM

In summary, we have successfully developed a weakly donor-acceptor-donor  $\pi$ -conjugated system featuring isomerism-dependent RTP characteristics. The substitution mode exerted a notable influence on molecular planarity and  $\pi$ -conjugation, enabling precise control over the excited-state characteristics. Down-lying upper triplet excited states introduce additional TA-ISC channels as revealed by theoretical investigations and proved by temperature-dependent photoluminescence and fs-and ns-transient absorption spectra. As a result, the overall ISC rate constant has reached a remarkable value of  $1.93{\times}10^9~{\rm s}^{-1}$ . It is worth noting that the principle of TA-ISC is in its infancy, but it is a practical mechanism for developing novel RTP materials and deserves further investigation.

#### **Conflicts of interest**

There are no conflicts to declare.

#### **Author contributions**

View Article Online DOI: 10.1039/D5SC07119D

W.H. performed all photophysical measurements, analysed data, synthesized materials, and grew the crystals. Z.Y. and C.W. performed the theoretical calculations. K.Z. assisted in the analysis of molecular crystal structure. Z.H. and Q.Z. designed and supervised the research and wrote the paper. All authors discussed the results and commented on the manuscript.

#### Data availability

The data that support the findings of this study are available in the Electronic Supplementary Information.

#### **Acknowledgements**

The authors acknowledge the financial support by the National Natural Science Foundation of China (No. 22375054 and No. 21975061), the Natural Science Foundation of Guangdong Province (No. 2024B15150200960), the Shenzhen Fundamental Research Program (No. JCYJ20241202152659001 and No. GXWD20231130104319001), and the Postdoctoral Fellowship Program (Grade C) of China Postdoctoral Science Foundation (No. GZC20252722). The authors thank Dr. Kang Zhou (Shenzhen Polytechnic University) for single-crystal structure analysis.

#### References

- W. Zhao, Z. He and B. Z. Tang, Room-temperature phosphorescence from organic aggregates, *Nat. Rev. Mater.*, 2020, 5, 869-885.
- B. Zhou and D. Yan, Long Persistent Luminescence from Metal-Organic Compounds: State of the Art, Adv. Funct. Mater., 2023, 33, 2300735.
- W. Huang and Z. He, Initialing circularly polarized roomtemperature phosphorescence from purely organic luminophore aggregate, Synlett, 2023, 34, 2249-2256.
- 4. S. M. A. Fateminia, Z. Mao, S. Xu, Z. Yang, Z. Chi and B. Liu, Organic Nanocrystals with Bright Red Persistent Room-Temperature Phosphorescence for Biological Applications, *Angew. Chem. Int. Ed.*, 2017, **56**, 12160-12164.
- Z. Tian, D. Li, E. V. Ushakova, V. G. Maslov, D. Zhou, P. Jing, D. Shen, S. Qu and A. L. Rogach, Multilevel Data Encryption Using Thermal-Treatment Controlled Room Temperature Phosphorescence of Carbon Dot/Polyvinylalcohol Composites, Adv. Sci., 2018, 5, 1800795.
- H. F. Higginbotham, M. Okazaki, P. de Silva, S. Minakata, Y. Takeda and P. Data, Heavy-Atom-Free Room-Temperature Phosphorescent Organic Light-Emitting Diodes Enabled by Excited States Engineering, ACS Appl. Mater. Interfaces, 2021. 13, 2899-2907.
- 7. Z. Wu, J. Nitsch and T. B. Marder, Persistent Room-Temperature Phosphorescence from Purely Organic Molecules and Multi-Component Systems, *Adv. Opt. Mater.*, 2021, **9**, 2100411.
- 8. N. Gan, X. Zou, M. Dong, Y. Wang, X. Wang, A. Lv, Z. Song, Y. Zhang, W. Gong, Z. Zhao, Z. Wang, Z. Zhou, H. Ma, X. Liu, Q. Chen, H. Shi, H. Yang, L. Gu, Z. An and W. Huang, Organic

This article is licensed under a Creative Commons Attribution-NonCommercial 3.0 Unported Licence

Open Access Article. Published on 10 November 2025. Downloaded on 11/11/2025 6:01:23 PM

**ARTICLE** 

Journal Name

phosphorescent scintillation from copolymers by X-ray irradiation, *Nat. Commun.*, 2022, **13**, 3995.

- Z. Huang, Z. He, B. Ding, H. Tian and X. Ma, Photoprogrammable Circularly Polarized Phosphorescence Switching of Chiral Helical Polyacetylene Thin Films, *Nat. Commun.*, 2022, 13, 7841.
- W. Shao and J. Kim, Metal-free organic phosphors toward fast and efficient room-temperature phosphorescence, Acc. Chem. Res., 2022, 55, 1573-1585.
- 11. H. Shi, W. Yao, W. Ye, H. Ma, W. Huang and Z. An, Ultralong Organic Phosphorescence: From Material Design to Applications, *Acc. Chem. Res.*, 2022, **55**, 3445-3459.
- 12. R. R. Valiev, V. N. Cherepanov, R. T. Nasibullin, D. Sundholm and T. Kurten, Calculating rate constants for intersystem crossing and internal conversion in the Franck-Condon and Herzberg-Teller approximations, *Phys. Chem. Chem. Phys.*, 2019, **21**, 18495-18500.
- M. Lv, Y. Yu, M. E. Sandoval-Salinas, J. Xu, Z. Lei, D. Casanova, Y. Yang and J. Chen, Engineering the Charge-Transfer State to Facilitate Spin-Orbit Charge Transfer Intersystem Crossing in Spirobis[anthracene]diones, Angew. Chem. Int. Ed., 2020, 59, 22179-22184.
- C. M. Marian, Understanding and Controlling Intersystem Crossing in Molecules, Annu. Rev. Phys. Chem., 2021, 72, 617-640.
- B. Wu, H. Su, A. Cheng, X. Zhang, T. Wang and G. Zhang, The El-Sayed's rule analogy enables long-lived room temperature phosphorescence in twisted biphenyls, *Cell Rep. Phys. Sci.*, 2023, 4, 101245.
- Y. He, J. Wang, Q. Li, S. Qu, C. Zhou, C. Yin, H. Ma, H. Shi, Z. Meng and Z. An, Highly Efficient Room-Temperature Phosphorescence Promoted via Intramolecular-Space Heavy-Atom Effect, Adv. Opt. Mater., 2023, 11, 2201641.
- Y. Zhou, L. Qu, S. Yi, C. Wang, X. Chen, S. Tang, H. Tang, Y. Li, K. Wang, Y. Zhao and C. Yang, Dual Promotion of Phosphorus Groups for Ultralong Room Temperature Phosphorescence with High Efficiency, Adv. Opt. Mater., 2022, 11, 2201904.
- S. Kuno, T. Kanamori, Z. Yijing, H. Ohtani and H. Yuasa, Long Persistent Phosphorescence of Crystalline Phenylboronic Acid Derivatives: Photophysics and a Mechanistic Study, ChemPhotoChem, 2017, 1, 102-106.
- J. T. Buck, A. M. Boudreau, A. DeCarmine, R. W. Wilson, J. Hampsey and T. Mani, Spin-Allowed Transitions Control the Formation of Triplet Excited States in Orthogonal Donor-Acceptor Dyads, Chem, 2019, 5, 138-155.
- L. Zhang, M. Li, Q.-Y. Gao and C.-F. Chen, An ultralong room-temperature phosphorescent material based on the combination of small singlet—triplet splitting energy and Haggregation, Chem. Commun., 2020, 56, 4296-4299.
- M. Park, H. S. Kim, H. Yoon, J. Kim, S. Lee, S. Yoo and S. Jeon, Controllable Singlet-Triplet Energy Splitting of Graphene Quantum Dots through Oxidation: From Phosphorescence to TADF, Adv. Mater., 2020, 32, 2000936.
- J. Yu, H. Ma, W. Huang, Z. Liang, K. Zhou, A. Lv, X. G. Li and Z. He, Purely Organic Room-Temperature Phosphorescence Endowing Fast Intersystem Crossing from Through-Space Spin-Orbit Coupling, *JACS Au*, 2021, 1, 1694-1699.
- M. K. Etherington, J. Gibson, H. F. Higginbotham, T. J. Penfold and A. P. Monkman, Revealing the spin-vibronic

fluorescence, *Nat. Commun.*, 2016p**7**)1368**0**9/D5SC07119D

Y. Wang, J. Yang, M. Fang, Y. Yu, B. Zou, L. Wang, Y. Tian, J. Cheng, B. Z. Tang and Z. Li, Förster Resonance Energy Transfer: An Efficient Way to Develop Stimulus-Responsive

coupling mechanism of thermally activated delayed

- Room-Temperature Phosphorescence Materials and Their Applications, *Matter*, 2020, **3**, 449-463.

  25. F.-F. Shen, Y. Chen, X. Dai, H.-Y. Zhang, B. Zhang, Y. Liu and Y. Liu, Purely organic light-harvesting phosphorescence
- Y. Liu, Purely organic light-harvesting phosphorescence energy transfer by β-cyclodextrin pseudorotaxane for mitochondria targeted imaging, *Chem. Sci.*, 2021, **12**, 1851-1857.
- W. Xie, W. Huang, J. Li, Z. He, G. Huang, B. S. Li and B. Z. Tang, Anti-Kasha triplet energy transfer and excitation wavelength dependent persistent luminescence from host-guest doping systems, *Nat. Commun.*, 2023, 14, 8098.
- Y. Tao, R. Chen, H. Li, J. Yuan, Y. Wan, H. Jiang, C. Chen, Y. Si, C. Zheng, B. Yang, G. Xing and W. Huang, Resonance-Activated Spin-Flipping for Efficient Organic Ultralong Room-Temperature Phosphorescence, *Adv. Mater.*, 2018, 30, 1803856.
- Y. Tao, C. Liu, Y. Xiang, Z. Wang, X. Xue, P. Li, H. Li, G. Xie, W. Huang and R. Chen, Resonance-Induced Stimuli-Responsive Capacity Modulation of Organic Ultralong Room Temperature Phosphorescence, *J. Am. Chem. Soc.*, 2022, 144, 6946-6953.
- S. Garain, S. Sarkar, B. Chandra Garain, S. K. Pati and S. J. George, Chiral Arylene Diimide Phosphors: Circularly Polarized Ambient Phosphorescence from Bischromophoric Pyromellitic Diimides, *Angew. Chem. Int. Ed.*, 2022, 61, e202115773.
- H. Su, K. Hu, W. Huang, T. Wang, X. Zhang, B. Chen, H. Miao,
   X. Zhang and G. Zhang, Functional Roles of Polymers in
   Room-Temperature Phosphorescent Materials:
   Modulation of Intersystem Crossing, Air Sensitivity and
   Biological Activity, Angew. Chem. Int. Ed., 2023, 62,
   e202218712.
- 31. W. Huang, C. Fu, Z. Liang, K. Zhou and Z. He, Strong Circularly-Polarized Room-Temperature Phosphorescence from a Feasibly Separable Scaffold of Bidibenzo[b,d]furan with Locked Axial Chirality, *Angew. Chem. Int. Ed.*, 2022, **61**, e202202977.
- 32. Q. Jia, X. Yan, B. Wang, J. Li, W. Xu, Z. Shen, C. Bo, Y. Li and L. Chen, Construction of room temperature phosphorescent materials with ultralong lifetime by in-situ derivation strategy, *Nat. Commun.*, 2023, **14**, 7164.
- B33. E. Bassan, A. Gualandi, P. G. Cozzi and P. Ceroni, Design of BODIPY dyes as triplet photosensitizers: electronic properties tailored for solar energy conversion, photoredox catalysis and photodynamic therapy, *Chem. Sci.*, 2021, **12**, 6607-6628.
- Y. Dong, A. Elmali, J. Zhao, B. Dick and A. Karatay, Long-Lived Triplet Excited State Accessed with Spin-Orbit Charge Transfer Intersystem Crossing in Red Light-Absorbing Phenoxazine-Styryl BODIPY Electron Donor/Acceptor Dyads, ChemPhysChem, 2020, 21, 1388-1401.
- Y. Zhang, Q. Sun, J. Chen, S. Cui, H. Zhang, S. Xue and W. Yang, Evoking ultra-long molecular room temperature phosphorescence of pure carbazole derivatives, *Chem. Eng. J.*, 2022, 447, 137458.

ARTICLE Journal Name

- S. Garain, S. N. Ansari, A. A. Kongasseri, B. Chandra Garain,
   S. K. Pati and S. J. George, Room temperature charge-transfer phosphorescence from organic donor-acceptor Co-crystals, *Chem. Sci.*, 2022, 13, 10011-10019.
- W. Huang, Y. Zhu, K. Zhou, L. Chen, Z. Zhao, E. Zhao and Z. He, Boosting Circularly Polarized Luminescence from Alkyl-Locked Axial Chirality Scaffold by Restriction of Molecular Motions, Chem. - Eur. J., 2024, 30, e202303667.
- J. Ma, X. Zhang and D. L. Phillips, Time-Resolved Spectroscopic Observation and Characterization of Water-Assisted Photoredox Reactions of Selected Aromatic Carbonyl Compounds, Acc. Chem. Res., 2019, 52, 726-737.
- 39. J. Zhou, L. Stojanović, A. A. Berezin, T. Battisti, A. Gill, B. M. Kariuki, D. Bonifazi, R. Crespo-Otero, M. R. Wasielewski and Y.-L. Wu, Organic room-temperature phosphorescence from halogen-bonded organic frameworks: hidden electronic effects in rigidified chromophores, Chem. Sci., 2021, 12, 767-773.
- 40. Y. Ma, Y. Yu, J. Li, S. Liu, W. Huang and Q. Zhao, Stimuli-responsive photofunctional materials for green and security printing, *InfoMat*, 2021, **3**, 82-100.
- H. Uoyama, K. Goushi, K. Shizu, H. Nomura and C. Adachi, Highly efficient organic light-emitting diodes from delayed fluorescence, *Nature*, 2012, 492, 234-238.
- Y. Wada, H. Nakagawa, S. Matsumoto, Y. Wakisaka and H. Kaji, Organic light emitters exhibiting very fast reverse intersystem crossing, *Nat. Photonics*, 2020, 14, 643-649.
- L. Deng, Z. Ma, J. Zhou, L. Chen, J. Wang, X. Qiao, D. Hu, D. Ma, J. Peng and Y. Ma, Regulating excited state of sulfone-locked triphenylamine heteroaromatics for high-efficiency ultralong room-temperature phosphorescence, *Chem. Eng. J.*, 2022, 449, 137834.
- 44. H. Yang, Y. Wang, X. Yao, H. Ma, J. Yu, X. Li, X. Wang, X. Liang, Q. Peng, S. Cai, Z. An and W. Huang, Efficient and Ultralong Room Temperature Phosphorescence from Isolated Molecules under Visible Light Excitation, J. Am. Chem. Soc., 2025, 147, 1474-1481.
- 45. Y. Xiao, J. Li, Z. Song, J. Liao, M. Shen, T. Yu and W. Huang, 3D Printable Materials with Visible Light Triggered Photochromism and Room Temperature Phosphorescence, *J. Am. Chem. Soc.*, 2025, **147**, 20372-20380.
- 46. R. G. Bennett and P. J. McCartin, Radiationless Deactivation of the Fluorescent State of Substituted Anthracenes, *J. Chem. Phys.*, 1966, **44**, 1969-1972.
- X. Han, H.-Q. Zheng, Y. Yang, Y. Cui and G. Qian, Tunable Room-Temperature Phosphorescence in Hydrogen-Bonded Organic Crystals via H-Bonding Units, Adv. Funct. Mater., 2025, 35, 2425934.
- 48. D. Dou, X. Zhou, T. Wang, Q. Yang, X. Tan, Z. Ling, M. Manz, X. Liu, G.-J. A. H. Wetzelaer, X. Li, M. Baumgarten, P. W. M. Blom and Y. Li, Intramolecular Through-Space Charge-Transfer Effect for Achieving Room-Temperature Phosphorescence in Amorphous Film, Adv. Opt. Mater., 2024, 12, 2400976.
- 49. X. Liu, L. Yang, X. Li, L. Zhao, S. Wang, Z.-H. Lu, J. Ding and L. Wang, An Electroactive Pure Organic Room-Temperature Phosphorescence Polymer Based on a Donor-Oxygen-Acceptor Geometry, *Angew. Chem. Int. Ed.*, 2021, **60**, 2455-2463.
- 50. T. Wang, Z. Hu, X. Nie, L. Huang, M. Hui, X. Sun and G. Zhang, Thermochromic aggregation-induced dual

- phosphorescence via temperature-dependent, sp3-lighed donor-acceptor electronic coupling. Nato. Communic., 2021, 12, 1364.
- 51. W. Huang, Y. Zhu, X. Xie, G. Tang, K. Zhou, L. Song and Z. He, Utilizing weakly donor-acceptor ternary pi-conjugated architecture to achieve single-component white luminescence and stimulus-responsive room-temperature phosphorescence, *Chem. Sci.*, 2024, **15**, 12316-12325.
- W. Dai, X. Niu, X. Wu, Y. Ren, Y. Zhang, G. Li, H. Su, Y. Lei, J. Xiao, J. Shi, B. Tong, Z. Cai and Y. Dong, Halogen Bonding: A New Platform for Achieving Multi-Stimuli-Responsive Persistent Phosphorescence, *Angew. Chem. Int. Ed.*, 2022, 61, e202200236.
- Z. Wu, J. Nitsch, J. Schuster, A. Friedrich, K. Edkins, M. Loebnitz, F. Dinkelbach, V. Stepanenko, F. Würthner, C. M. Marian, L. Ji and T. B. Marder, Persistent Room Temperature Phosphorescence from Triarylboranes: A Combined Experimental and Theoretical Study, *Angew. Chem. Int. Ed.*, 2020, 59, 17137-17144.
- C. Chen, Z. Chi, K. C. Chong, A. S. Batsanov, Z. Yang, Z. Mao,
   Z. Yang and B. Liu, Carbazole isomers induce ultralong organic phosphorescence, *Nat. Mater.*, 2021, 20, 175-180.
- 55. J. Song, Y. Wang, L. Qu, L. Fang, X. Zhou, Z.-X. Xu, C. Yang, P. Wu and H. Xiang, Room-Temperature Phosphorescence of Pure Axially Chiral Bicarbazoles, *J. Phys. Chem. Lett*, 2022, **13**, 5838-5844.
- S. H. Jeong and J. Y. Lee, Dibenzothiophene derivatives as host materials for high efficiency in deep blue phosphorescent organic light emitting diodes, *J. Mater. Chem.*, 2011, 21,14604-14609.
- X. Yao, H. Ma, X. Wang, H. Wang, Q. Wang, X. Zou, Z. Song, W. Jia, Y. Li, Y. Mao, M. Singh, W. Ye, J. Liang, Y. Zhang, Z. Liu, Y. He, J. Li, Z. Zhou, Z. Zhao, Y. Zhang, G. Niu, C. Yin, S. Zhang, H. Shi, W. Huang and Z. An, Ultralong organic phosphorescence from isolated molecules with repulsive interactions for multifunctional applications, Nat. Commun., 2022, 13, 4890.
- H. Wu, W. Chi, Z. Chen, G. Liu, L. Gu, A. K. Bindra, G. Yang,
   X. Liu and Y. Zhao, Achieving Amorphous Ultralong Room
   Temperature Phosphorescence by Coassembling Planar
   Small Organic Molecules with Polyvinyl Alcohol, Adv. Funct.
   Mater., 2019, 29, 1807243.
- 59. Y. Zhou, W. Qin, C. Du, H. Gao, F. Zhu and G. Liang, Long-Lived Room-Temperature Phosphorescence for Visual and Quantitative Detection of Oxygen, *Angew. Chem. Int. Ed.*, 2019, **58**, 12102-12106.
- 60. Z. Liang, M. Wei, S. Zhang, W. Huang, N. Shi, A. Lv, H. Ma and Z. He, Activating Molecular Room-Temperature Phosphorescence by Manipulating Excited-State Energy Levels in Poly(vinyl alcohol) Matrix, ACS Appl. Mater. Interfaces, 2023, 15, 35534-35542.
- H. Ma, Q. Peng, Z. An, W. Huang and Z. Shuai, Efficient and Long-Lived Room-Temperature Organic Phosphorescence: Theoretical Descriptors for Molecular Designs, J. Am. Chem. Soc., 2019, 141, 1010-1015.
- 62. N. Aizawa, Y.-J. Pu, Y. Harabuchi, A. Nihonyanagi, R. Ibuka, H. Inuzuka, B. Dhara, Y. Koyama, K.-i. Nakayama, S. Maeda, F. Araoka and D. Miyajima, Delayed fluorescence from inverted singlet and triplet excited states, *Nature*, 2022, 609, 502-506.
- H. Noda, X.-K. Chen, H. Nakanotani, T. Hosokai, M. Miyajima, N. Notsuka, Y. Kashima, J.-L. Brédas and C.

Journal Name ARTICLE

View Article Online DOI: 10.1039/D5SC07119D

**Shemical Science Accepted Manuscript** 

- Adachi, Critical role of intermediate electronic states for spin-flip processes in charge-transfer-type organic molecules with multiple donors and acceptors, *Nat. Mater.*, 2019, **18**, 1084-1090.
- 64. A. L. Schleper, K. Goushi, C. Bannwarth, B. Haehnle, P. J. Welscher, C. Adachi and A. J. C. Kuehne, Hot exciplexes in U-shaped TADF molecules with emission from locally excited states, *Nat. Commun.*, 2021, **12**, 6179.
- 65. B. Li, J. Lou, H. Zhang, G. Li, X. He, Y. Huang, N. Zheng, Z. Wang, D. Ma and B. Z. Tang, "Exciton Recovery" Strategy in Hot Exciton Emitter toward High-Performance Non-Doped Deep-Blue and Host-Sensitized Organic Light-Emitting Diodes, *Adv. Funct. Mater.*, 2023, **33**, 2212876.
- Y. Yang, F. Geng, Z. Jiang, Y. Liu, T. Guan, C. Qin, C. Zhuang and Y. Liu, Ultrafast dynamics of mCP and Br-mCP: Insights from transient absorption spectroscopy, *J. Lumin.*, 2025,
- 67. Y. Yang, Z. Jiang, Y. Liu, T. Guan, Q. Zhang, C. Qin, K. Jiang and Y. Liu, Transient Absorption Spectroscopy of a Carbazole-Based Room-Temperature Phosphorescent Molecule: Real-Time Monitoring of Singlet-Triplet Transitions, J. Phys. Chem. Lett, 2022, 13, 9381-9389.

View Article Online DOI: 10.1039/D5SC07119D

## Data availability statements

The data supporting this article, including materials, instruments, synthetic and experimental procedures, and characterization data have been included in Electronic Supplementary Information.